

Bimodal Waveguide Interferometer RI Sensor Fabricated on Low-Cost Polymer Platform

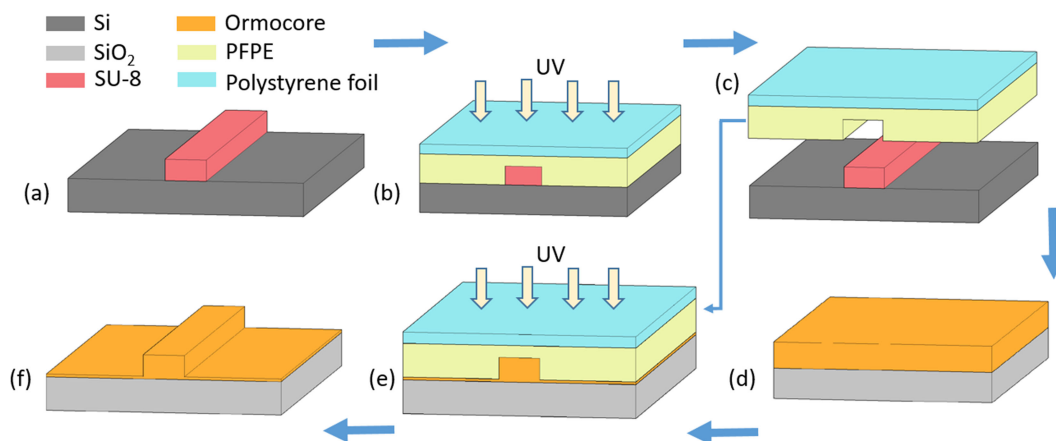
Volume 11, Number 2, April 2019

Yuxin Liang

Mingshan Zhao, *Member, IEEE*

Zhenlin Wu, *Member, IEEE*




Geert Morthier, *Senior Member, IEEE*



DOI: 10.1109/JPHOT.2019.2900741

1943-0655 © 2019 IEEE

Bimodal Waveguide Interferometer RI Sensor Fabricated on Low-Cost Polymer Platform

Yuxin Liang ^{1,2}, Mingshan Zhao ² *Member, IEEE*,
Zhenlin Wu,² *Member, IEEE*,
and Geert Morthier ¹ *Senior Member, IEEE*

¹Photonics Research Group, Department of Information and Technology, Ghent University, Ghent 9000, Belgium

²School of Physics and Optoelectronic Engineering, Dalian University of Technology, Dalian 116023, China

DOI:10.1109/JPHOT.2019.2900741

1943-0655 © 2019 IEEE. Translations and content mining are permitted for academic research only. Personal use is also permitted, but republication/redistribution requires IEEE permission. See http://www.ieee.org/publications_standards/publications/rights/index.html for more information.

Manuscript received February 13, 2019; accepted February 18, 2019. Date of publication February 21, 2019; date of current version March 8, 2019. This work was supported in part by CSC scholarship, in part by 111 Project (BC2018008), in part by the International Science & Technology Cooperation Program of China under Grant 2014DFG32590, in part by the Fundamental Research Funds for the Central Universities Natural Science Foundation of China under Grant 61704017, in part by the Petro China Innovation Foundation under Grant 2016D-5007-0603, in part by the Fundamental Research Funds for the Central Universities under Grants DUT18ZD106, DUT18GF102, and DUT18LAB20, and in part by the Dalian Science and Technology Innovation Foundation under Grant 2018J11CY006. Corresponding author: Mingshan Zhao (e-mail: mszhao@dlut.edu.cn).

Abstract: A refractive index sensor based on bimodal waveguide interferometer is demonstrated on the low-cost polymer platform for the first time. Different from conventional interferometers which make use of the interference between the light from two arms, bimodal waveguide interferometers utilize the interference between the two different internal modes in the waveguide. Since the utilized first higher mode has a wide evanescent tail which interacts with the external environment, the interferometer can reach a high sensitivity. Instead of vertical bimodal structure which is normally employed, the lateral bimodal waveguide is adopted in order to simplify the fabrication process. A unique offset between the centers of single mode waveguide and bimodal waveguide is designed to excite the two different modes with equal power which contributes to the maximum fringe visibility. The bimodal waveguide interferometer is finally fabricated on optical polymer (Ormocore) which is transparent at both infrared and visible wavelengths. It is fabricated using the UV-based soft imprint technique which is simple and reproducible. The bulk sensitivity of fabricated interferometer sensor with a 5 mm sensing length is characterized using different mass concentration sodium chloride solutions. The sensitivity is obtained as 316π rad/RIU and the extinction ratio can reach 18 dB.

Index Terms: Refractive index sensor, bimodal waveguide interferometer, polymer waveguide, nanoimprint technique.

1. Introduction

The refractive index (RI) sensors are the fundamental devices in the sensing area. By introducing different mediums, RI sensor can be applied in various fields such as Biology Engineering, Medical Science and Environmental Science. In recent years, integrated photonic RI sensors have attracted

increasing attention due to their advantages such as high sensitivity, miniature dimensions, mechanical stability and immunity to electromagnetic interference [1], [2]. Moreover, label-free and real-time monitoring can also be realized. Integrated photonic RI sensors are normally based on the evanescent tail of waveguide modes and various structures have been demonstrated such as Mach-Zehnder interferometers (MZIs) [3], Young interferometers [4], microring resonators [5]–[7], photonic crystals [8], [9] and plasmonic structures [10], [11]. Interferometer RI sensors which have been studied from the beginning still stay vigorous due to the advantages such as high sensitivity and small limit of detection (LOD) [12]. The LOD can reach 10^{-8} of refractive index unit (RIU) which is two orders of the that of plasmonic structure based RI sensors [13].

For conventional interferometer RI sensors, the interference is normally obtained between the light from two channels: a reference channel and a sensing channel. The sensing channel can feel the environment change and then modulates the output power after the interference. In order to prevent the coupling between the two channels, enough spatial separation is necessary. Interferometer RI sensors have been demonstrated on many waveguide structures, such as strip and rib waveguides [14], arrow waveguides [15], plasmonic waveguides [16], slot waveguides [17], and nanoporous materials based waveguides [18]. Recently a novel waveguide structure, a bimodal waveguide based interferometer was proposed. Unlike conventional interferometer RI sensors, the interference of bimodal waveguide interferometer occurs between the two modes of the bimodal waveguide: the fundamental mode and the first higher mode. Different from conventional interferometer RI sensors, both modes are affected by the external environment. However, the effects on the two modes are different which leads to an accumulated phase difference and finally modulates the output power. As the utilized first higher mode has a large evanescent tail which is the part of the mode interacting with the environment, a high sensitivity can be reached. A vertical bimodal interferometer was proposed in [19]. The interference is obtained between fundamental mode and the first vertical higher mode. The output power is then received and analyzed by the photodetector which is placed close to the output port of the bimodal waveguide. There are still some disadvantages for this kind of bimodal interferometer. As there is a height gap between the single mode part and the vertical bimodal waveguide part, two lithography and etching steps are required. Moreover, as the photodetector should be placed close to the bimodal waveguide output port, packaging will be a problem. In order to address these problems, a horizontal bimodal interferometer has been proposed [20]. The fabrication process becomes much simpler as just one lithography and etching step are needed. In addition, a single waveguide is designed to export the light out which makes it easy to connect with fiber or vertical grating coupler, which itself can simplify the packaging. Besides, as the first higher mode distributes laterally, the evanescent wave mostly exists on the top of the waveguide. That makes it very suitable for bonding biomolecules which is normally needed in specific detection. Moreover, as the position of the single mode waveguide can be adjusted to the lateral bimodal waveguide interferometer, the power ratio of the different excited modes can be controlled which will make it easy to obtain maximum fringe visibility.

Polymer as optical material has attracted a lot of attention for decades due to its many advantages [21], [22]. Among those, the most attractive one is the fact that different optical properties such as low loss and high electro-optic coefficient can be realized by operating on the molecular scale [23], [24]. Moreover, polymer is usually transparent at both infrared (1300–1550 nm) and visible wavelengths. The transparency at short wavelengths makes it preferred for biosensing and chemical sensing, as the absorption loss of water at short wavelengths is much lower than at infrared wavelengths. In this paper, the fabricated device works at the wavelength range: 890–910 nm instead of the infrared wavelengths in order to decrease the absorption loss. Several novel fabrication processes such as direct laser writing [25] and nanoimprint lithography (NIL) [26] have already been developed. UV-based soft nanoimprint lithography (Soft UV NIL) is an improved version of NIL [27]. As UV curing is adopted, high temperature and pressure are no longer needed. Moreover, high-resolution nanopatterns down to 50 nm resolution on a large scale can be achieved with low-cost equipment [28].

In this article, a lateral bimodal interferometer RI sensor based on the polymer platform is demonstrated for the first time. The two lateral modes in the bimodal waveguide are utilized to constitute

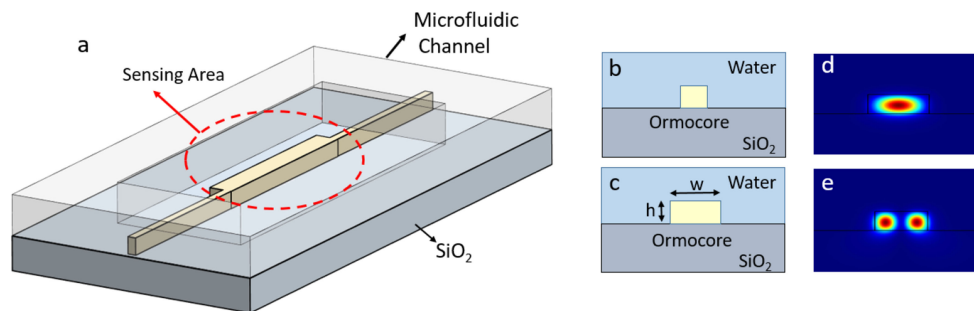


Fig. 1. (a) Schematic of the bimodal interferometer RI sensor. (b) Input/output single mode waveguide cross-section. (c) Bimodal waveguide cross-section. (d) Fundamental mode of the bimodal waveguide. (e) First higher mode of the bimodal waveguide.

the interferometer. The power of the two different modes reaches the same value by a simple design of the single mode waveguide position. The RI sensor is finally fabricated by a simple and reproducible technique, Soft UV NIL. The bulk sensitivity of the RI sensor with a 5 mm sensing length is characterized using sodium chloride (NaCl) solutions and the sensitivity and extinction ratio are obtained as 316π rad/RIU and 18 dB respectively.

2. Principle and Design

The schematic of the bimodal waveguide interferometer is illustrated in Fig. 1(a). The interferometer can be divided into three sections. The bimodal waveguide which supports two lateral modes is located in the center. Two single mode waveguides constitute the input and output waveguides at the two sides of the bimodal waveguide. Since the large lateral dimension affords the two different modes, all the sections have the same thickness, which simplifies the fabrication process. On top of the chip, a microfluidic channel is bonded to lead the analyte solution flow above the sensing area. The cross-section structures of the single mode waveguide and the bimodal waveguide are illustrated in Fig. 1(a) and (b). The two modes of the bimodal waveguide are calculated using a bidirectional eigenmode expansion solver (Mode Solution package from Lumerical Solutions, Inc) and illustrated in the Fig. 1(d) and (e). Ormocore (Microresist Technology) as a commercial optical material is adopted and the refractive index (RI) is 1.543 at the wavelength of 890 nm. The under cladding layer is SiO₂ with the RI of 1.453 at this wavelength. The top cladding is assumed to be water during the simulation since water is normally employed as solution in the biosensing and chemical sensing and the RI is 1.33. Only the transverse-electric (TE) mode is considered, but the transverse-magnetic (TM) mode works similarly. Both the width and height of the single mode waveguide are designed to be 1 μm so that the single mode condition can be guaranteed. The width of the bimodal waveguide is designed as 2 μm in order to support lateral two modes.

The principle of the bimodal waveguide interferometer is similar to that of the MZI structures. The difference is that the interference occurs between the two internal modes instead of between the light coming from the two arms. The light is first launched into the input waveguide and then coupled to the two lateral modes (E_{11}^x and E_{12}^x) and radiation modes supported by the bimodal waveguide at the discontinuous junction. The power ratio of the E_{11}^x mode and E_{12}^x mode can be adjusted by controlling the input waveguide location. Both the two lateral modes propagate through the sensing area with different velocities and the phase difference accumulates before interference at the second discontinuous junction. As the two modes are affected differently from the environment, the accumulated phase different changes with the RI of the environment. Therefore, the change in RI of the environment can be traced via the shift in the transmission spectrum of the interferometer. The output power can be expressed as:

$$I_{out} = \frac{1}{2} \left(I_0 + I_1 + 2\sqrt{I_0 I_1} \cos(\Delta\varphi) \right) \quad (1)$$

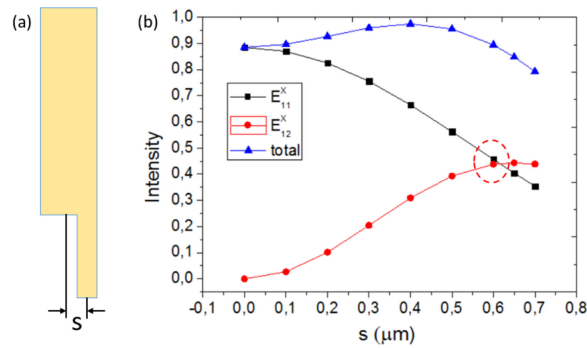


Fig. 2. (a) Schematic of the discontinuous junction between the single mode waveguide and the bimodal waveguide. (b) The dependence of the E_{11}^x mode and the E_{12}^x mode power, and the total power on the offset between the centers of the bimodal waveguide and the single mode waveguide.

where I_0 , I_1 and I_{out} are the power of the E_{11}^x mode and the E_{12}^x mode and the output power, respectively. $\Delta\varphi$ is the accumulated phase difference between the two incident modes after propagating through the sensing area. Two important parameters for interferometer RI sensors to be considered are sensitivity and fringe visibility. The sensitivity can be improved by increasing the length of the sensing area. The fringe visibility indicates the contrast of the interference pattern which influences the measurement accuracy. The fringe visibility, γ , can be expressed as:

$$\gamma = \frac{2\sqrt{I_0 I_1}}{I_0 + I_1} \quad (2)$$

From the Formula (2), it can be seen that γ reaches maximum when each mode has identical power. The power ratio of two different modes can only be controlled by adjusting the input waveguide location when the dimensions of both single mode waveguide and bimodal waveguide are fixed.

The detailed structure of the discontinuous junction is illustrated in the Fig. 2(a). The power of the E_{11}^x mode and the E_{12}^x mode propagating in the bimodal waveguide excited by the discontinuous junction is simulated using an FDTD software package (Lumerical Solutions, Inc). The Fig. 2(b) shows the dependence of total power and both the internal modes' power on the offset between the centers of the single mode waveguide and the bimodal waveguide. It can be seen that only the fundamental mode is excited when $s = 0 \mu\text{m}$. That is because only even modes can be excited when the input mode is in the middle of the bimodal waveguide according to the self-imaging principle [29]. The E_{12}^x mode power increases with the increasing s while the E_{11}^x mode power exhibits the reverse relationship. At about $s = 0.6 \mu\text{m}$, the powers of the two lateral modes reach the same value which will lead to maximal fringe visibility. The Fig. 2(b) also shows that there is always some power coupled to the radiation modes and about 10% power is lost at the discontinuous junction when $s = 0.6 \mu\text{m}$.

3. Fabrication

The bimodal waveguide interferometer is fabricated by Soft UV NIL technique, which is considered cost-effective and productive. Since the nanoimprint technique is based on replication, the quality of the fabricated interferometer mainly depends on the quality of the master mold. The master mold in this article is fabricated by UV lithography using a negative photoresist, SU8-2 (MicroChemicals) which has been widely employed on master molds for many years. As no etching process is introduced, good roughness can be reached. The fabrication process is described below. First, an adhesion layer, Ti-prime (MicroChemicals), is spin-coated on the silicon wafer at 3000 r/min for 40 seconds and baked at 120 °C for 3 minutes. Then SU8-2 is spin-coated on the wafer at 5600 r/min for 40 seconds, followed by two steps of baking (65 °C for 2 minutes and 95 °C for 2 minutes). The

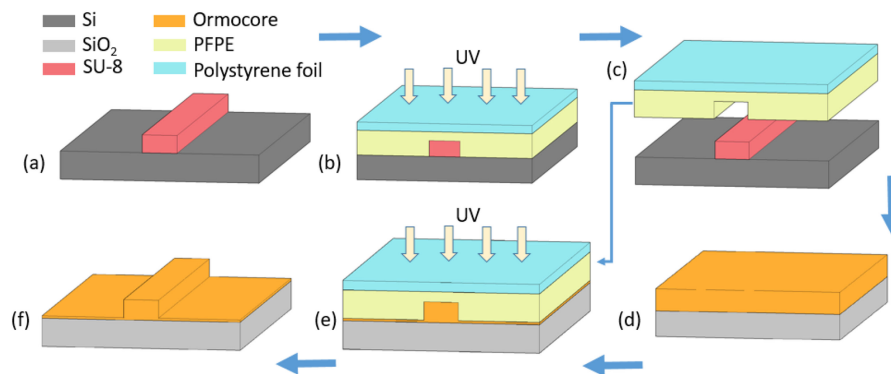


Fig. 3. Fabrication process of PFPE soft mode (a, b, c) and UV-based soft imprinting process (d, e, f).

film thickness is about 950 nm which is controlled by the spin-coating parameters. After exposure by the contact mask aligner, Süss MA6, the unexposed part is removed by about 40 seconds developing. Subsequently, a thermal reflow technique [30], which is considered as an effective way to smoothen the waveguide surfaces is applied.

PDMS has demonstrated its advantages in Soft UV NIL technique due to its characteristics such as flexible backbone structure, high degree of toughness and large elongation. However, its surface energy (25 mN/m) which is not low enough will cause damage to the master mold. Polytetrafluoroethylene (PFPE) has been demonstrated as a new material for the soft mold in the past years [31]. Its unique characteristics such as low surface energy and ideal elastic modulus have received a lot of attention. The fabrication of the soft mold is illustrated in Fig. 3(a), (b) and (c). The PFPE acrylate is prepared by mixing Irgacure 2022 photoinitiator (BASF) with Fluorolink MD 700 (Solvay Solexis) at the proportion 1:20. Then the mixture is cast on the top of SU8-2 master mold and covered by a Polystyrene foil on the top in order to improve the mechanical stability. Afterwards, a roller is employed to press and flatten the soft mold. Subsequent UV curing at 30 mW/cm² for 90 seconds is carried out. After being peeled off from the master mold, the PFPE soft mold is prepared. The nanoimprint process is shown in the Fig. 3(d), (e) and (f). First of all, an adhesion layer (OrmoPrime) is prepared on the SiO₂ on Si substrate which has been carefully cleared. The thickness of the SiO₂ layer is 3 μm so as to prevent the light leaking into the Si substrate. Then a thermal curing at 150 °C for 5 minutes is taking place. In order to obtain the designed height (1 μm) of the waveguide, Ormocore liquid is diluted by thinner maT in the proportion, 1:2.3. A filtration is also needed to remove the particles in the mixture. Afterwards, the Ormocore layer is prepared by spin-coating at 3000 r/min for 30 seconds and then baking at 120 °C for 10 minutes. Then the imprinting is done by carefully placing the PFPE soft mold on the sample. An extra flattening process is unnecessary as the capillary force is enough for the nanoimprinting. Subsequently, a UV curing with the intensity of 30 mW/cm² for 2 minutes is carried out in a nitrogen environment. Finally, a hard bake at 150 °C for 3 hours is applied after demolding the PFPE soft mold.

The fabricated bimodal waveguide interferometer is characterized by Nova 600 Nanolab SEM/FIB device, a dual beam instrument that combines a focused ion beam with an SEM which makes it easy for cross-section imaging. The SEM pictures of different parts of the bimodal interferometer are illustrated in Fig. 4. The cross-section of the single mode waveguide is shown in Fig. 4(a) and its width and height are 960 nm and 940 nm respectively. Fig. 4(b) and (c) show the cross-section and top view of the bimodal waveguide and a width of 1.96 μm is obtained. Both the widths of the single mode waveguide and the bimodal waveguide are slightly smaller than designed due to the replication. This problem can be resolved by designing a wider waveguide than needed. The discontinuous junction is illustrated in the Fig. 4(c) and (d). Fig. 4(c) is an aslant view of the discontinuous junction which clearly gives an idea of the concept and Fig. 4(d) shows the zoomed top view of the bimodal waveguide. It can be seen that the distance between the left side of the single mode waveguide and the right side of the bimodal waveguide is 2.1 μm and the center offset,

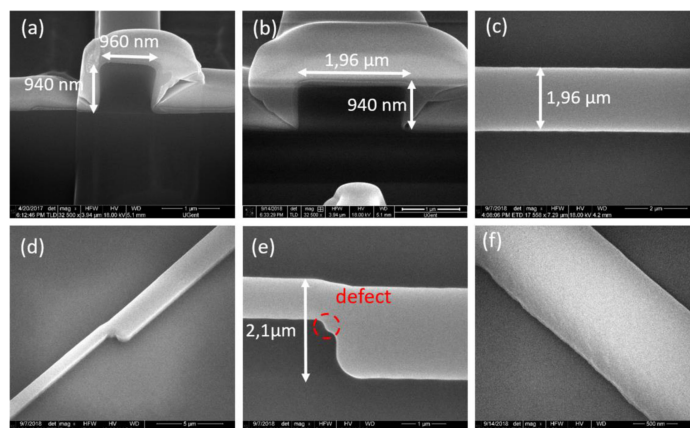


Fig. 4. SEM pictures of different parts of the fabricated polymer-based bimodal waveguide interferometer. (a) Cross-section of single mode waveguide. (b) Cross-section of bimodal waveguide. (c) Top view of the bimodal waveguide. (c) SEM picture of the discontinuous junction. (d) Zoomed SEM picture of the discontinuous junction. (e) Side wall of the waveguide. (f) SEM picture of the side wall of the waveguide.

0.6 μm which is the same as designed, can be obtained through a simple deduction. In spite of this high quality replication, there is still a small defect at the corner. This defect is replicated from the SU8-2 master mold, where it results from the fact that the lithography cannot fabricate the critical corner perfectly. The side wall of the waveguide is shown in Fig. 4(e) and low roughness can be observed. In general, this polymer-based bimodal interferometer RI sensor can be fabricated with a high quality using Soft UV NIL technique.

4. Experiment and Results

The spectrum of the fabricated RI sensor is characterized using a tunable laser (Newport, with a wavelength range: 890–910 nm and a resolution of 20 pm) and a power meter. In order to get a TE mode, a polarizer is placed between the tunable laser and the RI sensor chip. Lensed fibers are used to couple the light in and out of the RI sensor chip. A temperature controller is also applied in order to avoid the influence of the temperature changing. A microfluidic channel is also prepared to flow the analyte solution above the sensing area of the interferometer. It is fabricated using PDMS material and bonded on the chip using flip-chip equipment. For the purpose of the bulk RI sensing measurement, different mass concentration NaCl solutions (0%, 1%, 2%, 3%, 4%, 5%) are employed. As described in [32], 1% mass concentration leads to 1.7151×10^{-3} refractive index change. Since the effective indices of the two lateral modes are differently affected by the change of the analyte solution refractive index, the phase difference will be modulated by the change in the mass concentration and will thus affect the output spectrum. The measured output spectrum of different mass concentrations is depicted in Fig. 5(a).

In order to clearly show the spectrums of different mass concentrations, the curves have been shifted downwards by different values (0, 5, 10, 15, 20 dBm for the spectrum curves of the mass concentrations of 0%, 1%, 2%, 3%, 4% and 5% respectively). It can be clearly seen that the output spectrum shifts to the short wavelengths with the increasing of the mass concentration. The free spectral range (FSR) can be obtained as 5 nm and that the extinction ratio reaches 18 dB, implying a very good fringe visibility of the design. It also can be seen that the spectrum of the mass concentration, 5% deforms a little bit. This is because the RI of the solution is so large that the bimodal waveguide cannot support the first higher mode perfectly. Fig. 5(b) shows the wavelength shift as a function of the bulk RI change. After linear fitting, the sensitivity can be obtained as 789 nm/RIU. For interferometer RI sensors, the sensitivity is usually expressed in rad/RIU. After a simple mathematical derivation, the sensitivity of 316π rad/RIU can be obtained.

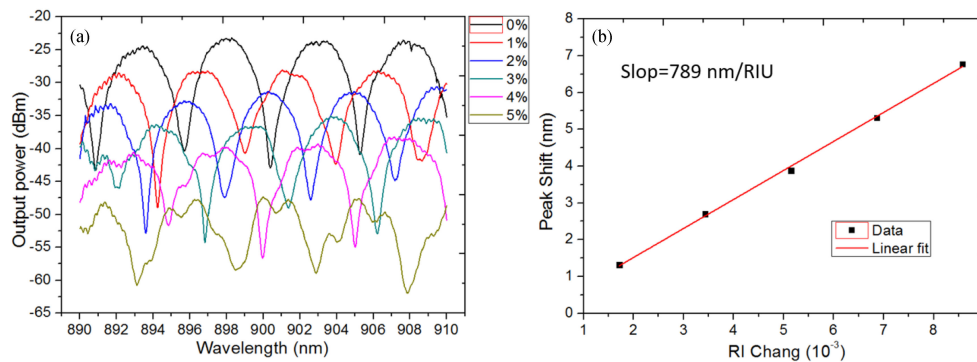


Fig. 5. (a) Output spectrums of different mass concentrations. (b) Peak shift versus RI changing and linear fit of the data.

We also compare with other reported bimodal interferometer RI sensors. In the article [33], a silicon based vertical bimodal interferometer is demonstrated, with a high sensitivity of 2026 rad/RIU or 645π rad/RIU. It is much higher than that demonstrated in our work. However, the sensor in [31] has a long sensing area (15 mm) which is 3 times larger than the length used in our work. A lateral bimodal interferometer is demonstrated on silicon in the article [20] with a sensitivity of 461.6π rad/RIU which is a little higher than that in our work. In conclusion, the polymer based lateral bimodal interferometer fabricated in this paper is still competitive.

5. Conclusions

A polymer-based bimodal waveguide interferometer RI sensor is demonstrated for the first time in this article. Unlike conventional interferometer RI sensors which utilize the interference between the light coming from two arms (reference arm and sensing arm), bimodal waveguide interferometers make use of the interference between the two internal modes in the bimodal waveguide. As the two modes are affected by the environment differently, the phase difference between the two modes is modulated by the external RI change which finally manifests itself in the transmission spectrum. For interferometer RI sensors, fringe visibility is an important parameter which will affect the measurement accuracy. Fringe visibility reaches maximum when the two internal modes get the same power. However, only fundamental mode can be excited when the single waveguide is placed in the middle of the bimodal waveguide due to the self-imaging principle. Therefore, the offset between the centers of the single mode waveguide and the bimodal waveguide is optimized to get the same power for the two modes. The polymer adopted in this article is Ormocore which has a large transparency window including infrared and visible wavelengths. Short wavelengths are preferred as the absorption loss from the water which is normally used as solution in the RI sensing is low. In this article, an 890 nm tunable laser is adopted instead of the communication wavelengths in order to decrease the absorption loss from the water. The bimodal waveguide interferometer is prepared using an easy and productive process, Soft UV NIL. A PDMS fluidic channel is also prepared and bonded on the chip using flip-chip equipment. The bulk sensitivity of the bimodal waveguide interferometer RI sensor with 5 mm sensing length is eventually characterized using different mass concentration NaCl solutions. A sensitivity as high as 316π rad/RIU is obtained and the extinction ratio reaches 18 dB. It is still competitive compared with the bimodal interferometer RI sensors fabricated on other optical materials. Taking into consideration the unique characteristics of the polymer, this approach is very promising for the future commercial exploitation.

References

- [1] X. Fan, I. M. White, S. I. Shopova, H. Zhu, J. D. Suter, and Y. Sun, "Sensitive optical biosensors for unlabeled targets: A review," *Analytica Chim. Acta*, vol. 620, pp. 8–26, 2008.

- [2] M. C. Estevez, M. Alvarez, and L. M. Lechuga, "Integrated optical devices for lab-on-a-chip biosensing applications," *Laser Photon. Rev.*, vol. 6, pp. 463–487, 2012.
- [3] B. J. Luff, J. S. Wilkinson, J. Piehler, U. Hollenbach, J. Ingenhoff, and N. Fabricius, "Integrated optical Mach-Zehnder biosensor," *J. Lightw. Technol.*, vol. 16, no. 4, pp. 583–592, Apr. 1998.
- [4] A. Ymeti *et al.*, "Fast, ultrasensitive virus detection using a young interferometer sensor," *Nano Lett.*, vol. 7, pp. 394–397, 2007.
- [5] K. D. Vos, I. Bartolozzi, E. Schacht, P. Bienstman, and R. Baets, "Silicon-on-insulator microring resonator for sensitive and label-free biosensing," *Opt. Exp.*, vol. 15, pp. 7610–7615, 2007.
- [6] N. A. Yebo, L. Petra, H. Zeger, and B. Roel, "An integrated optic ethanol vapor sensor based on a silicon-on-insulator microring resonator coated with a porous ZnO film," *Opt. Exp.*, vol. 18, pp. 11859–11866, 2010.
- [7] A. J. Qavi, J. T. Kindt, M. A. Gleeson, and R. C. Bailey, "Anti-DNA: RNA antibodies and silicon photonic microring resonators: Increased sensitivity for multiplexed microRNA detection," *Anal. Chem.*, vol. 83, pp. 5949–5956, 2011.
- [8] C. Kang, C. T. Phare, Y. A. Vlasov, S. Assefa, and S. M. Weiss, "Photonic crystal slab sensor with enhanced surface area," *Opt. Exp.*, vol. 18, pp. 27930–27937, 2010.
- [9] H. Lu *et al.*, "Integrated temperature sensor based on an enhanced pyroelectric photonic crystal," *Opt. Exp.*, vol. 21, pp. 16311–16318, 2013.
- [10] Y. Gao, Z. Xin, Q. Gan, X. Cheng, and F. J. Bartoli, "Plasmonic interferometers for label-free multiplexed sensing," *Opt. Exp.*, vol. 21, pp. 5859–5871, 2013.
- [11] D. J. Lee, H. D. Yim, S. G. Lee, and O. Bh, "Tiny surface plasmon resonance sensor integrated on silicon waveguide based on vertical coupling into finite metal-insulator-metal plasmonic waveguide," *Opt. Exp.*, vol. 19, pp. 19895–19900, 2011.
- [12] M. C. Estevez, M. Alvarez, and L. M. Lechuga, "Integrated optical devices for lab-on-a-chip biosensing applications," *Laser Photon. Rev.*, vol. 6, pp. 463–487, 2012.
- [13] H. Jirí, "Surface plasmon resonance sensors for detection of chemical and biological species," *Chem. Rev.*, vol. 39, pp. 462–493, 2010.
- [14] X. Jiang, Y. Chen, F. Yu, L. Tang, M. Li, and J.-J. He, "High-sensitivity optical biosensor based on cascaded Mach-Zehnder interferometer and ring resonator using Vernier effect," *Opt. Lett.*, vol. 39, pp. 6363–6366, 2014.
- [15] S.-H. Hsu and Y.-T. Huang, "A novel Mach-Zehnder interferometer based on dual-arrow structures for sensing applications," *J. Lightw. Technol.*, vol. 23, no. 12, pp. 4200–4206, 2005.
- [16] Y. Gao, Q. Gan, Z. Xin, X. Cheng, and F. J. Bartoli, "Plasmonic Mach-Zehnder interferometer for ultrasensitive on-chip biosensing," *ACS Nano*, vol. 5, pp. 9836–9844, 2011.
- [17] M. Hiltunen *et al.*, "Polymeric slot waveguide interferometer for sensor applications," *Opt. Exp.*, vol. 22, pp. 7229–7237, 2014.
- [18] K. Kim and T. E. Murphy, "Porous silicon integrated Mach-Zehnder interferometer waveguide for biological and chemical sensing," *Opt. Exp.*, vol. 21, pp. 19488–19497, 2013.
- [19] R. Levy and S. Ruschin, "Design of a single-channel modal interferometer waveguide sensor," *IEEE Sens. J.*, vol. 9, no. 2, pp. 146–151, Feb. 2009.
- [20] Q. Liu, K. W. Kim, Z. Gu, J. S. Kee, and M. K. Park, "Single-channel Mach-Zehnder interferometric biochemical sensor based on two-lateral-mode spiral waveguide," *Opt. Exp.*, vol. 22, pp. 27910–27920, 2014.
- [21] M. Rezem, A. Günther, B. Roth, E. Reithmeier, and M. Rahlves, "Low-cost fabrication of all-polymer components for integrated photonics," *J. Lightw. Technol.*, vol. 35, pp. 299–308, Jan. 2017.
- [22] F. Shi, N. Bamiedakis, P. P. Vasil'ev, R. V. Penty, I. H. White, and D. Chu, "Flexible multimode polymer waveguide arrays for versatile high-speed short-reach communication links," *J. Lightw. Technol.*, vol. 36, no. 13, pp. 2685–2693, Jul. 2018.
- [23] H. Ma, A. K. Y. Jen, and L. R. Dalton, "Polymer-based optical waveguides: Materials, processing, and devices," *Adv. Mater.*, vol. 14, pp. 1339–1365, 2010.
- [24] L. Eldada and L. W. Shacklette, "Advances in polymer integrated optics," *IEEE J. Sel. Topics Quantum Electron.*, vol. 6, no. 1, pp. 54–68, Jan./Feb. 2000.
- [25] E. Zraggen *et al.*, "Laser direct writing of single-mode polysiloxane optical waveguides and devices," *J. Lightw. Technol.*, vol. 32, no. 17, pp. 3036–3042, Sep. 2014.
- [26] R. Kirchner *et al.*, "Direct UV-imprinting of hybrid-polymer photonic microring resonators and their characterization," *J. Lightw. Technol.*, vol. 32, no. 9, pp. 1674–1681, May 2014.
- [27] S. J. Goh, H. J. M. Bastiaens, B. Vratzov, Q. Huang, F. Bijkerk, and K. J. Boller, "Fabrication and characterization of free-standing, high-line-density transmission gratings for the vacuum UV to soft X-ray range," *Opt. Exp.*, vol. 23, pp. 4421–4434, 2015.
- [28] N. Koo *et al.*, "Improved mold fabrication for the definition of high quality nanopatterns by soft UV-nanoimprint lithography using diluted PDMS material," *Microelectron. Eng.*, vol. 84, pp. 904–908, 2007.
- [29] L. B. Soldano and E. C. M. Pennings, "Optical multi-mode interference devices based on self-imaging: Principles and applications," *J. Lightw. Technol.*, vol. 13, no. 4, pp. 615–627, Apr. 1995.
- [30] C. Y. Chao and L. J. Guo, "Reduction of surface scattering loss in polymer microrings using thermal-reflow technique," *IEEE Photon. Technol. Lett.*, vol. 16, no. 6, pp. 1498–1500, Jun. 2004.
- [31] J. John, Y. Tang, J. P. Rothstein, J. J. Watkins, and K. R. Carter, "Large-area, continuous roll-to-roll nanoimprinting with PFPE composite molds," *Nanotechnology*, vol. 24, 2013, Art. no. 505307.
- [32] H. Su and X. G. Huang, "Fresnel-reflection-based fiber sensor for on-line measurement of solute concentration in solutions," *Sens. Actuators B Chem.*, vol. 126, pp. 579–582, 2007.
- [33] K. E. Zinoviev, A. B. González-Guerrero, C. Domínguez, and L. M. Lechuga, "Integrated bimodal waveguide interferometric biosensor for label-free analysis," *J. Lightw. Technol.*, vol. 29, no. 13, pp. 1926–1930, Jul. 2011.